Chapter 2

Embedded Fuzzy Logic Controllers in Electric Railway Transportation Systems

Stela Rusu-Anghel and Lucian Gherman

Additional information is available at the end of the chapter

http://dx.doi.org/10.5772/48588

1. Introduction

A. Power system harmonic pollution limitation using Fuzzy Logic controlled active filters

1.1. Introduction

Nonlinear loads system has been grooving on influence in electric power due to the advance of power electronics technologies. As a result, the harmonic pollution in the power system deteriorates the power quality significantly. One effect of the harmonic pollution is the harmonic resonance which may result in major voltage distortion in the power system.

1.1.1. Harmonic effect

The current harmonic components could cause the following problems:

- resonance effect with overvoltage and overcurrent consequences,
- additional losses,
- psophomentic disturbance of the telecommunication systems,
- disturbance in the remote control systems,
- malfunction of protection devices,
- misoperation of semiconductor-controllers.

The harmonic disturbance basically could be characterized by the individual (1) and total (2) harmonic distortion factors:

$$D_k = \frac{X_k}{X_1} \tag{1}$$

$$THD_X = \frac{\sqrt{\sum_{k=2}^{\infty} X^2{}_k}}{X_1} \tag{2}$$

where:

$k = \frac{f}{50Hz}$: the harmonic order;
X_k : k^{th} harmonic component of *I* or *V*;
X_i : fundamental frequency component of *I* or *V*

1.1.2. Psophometric interference

The high power lines could influence the neighbouring telecommunication networks by the following ways:

- Capacitive coupling: The voltage of the power line causes charging current ;
- Inductive coupling: The line current induces longitudinal emf.

The most dominant part of the psophometric noise is the inducing effect caused by the zero sequence components of the current. The power balance of the three-phase is near symmetrical during normal operation, thus the coupling is measurable only if the distance between the two systems is comparable with the phase distance of one system. However electric traction is a single-phase system with ground return and in consequence it is a natural zero sequence system. That is why it is important to calculate the psophometric noise. [1]

By telecommunication lines the rate of the disturbance could be characterized by the so called psophometric voltage. It could be calculated by this formula:

$$V_p = \sqrt{\sum_f \left(\frac{p_f}{p_{800}} \cdot V_f \right)^2} \tag{3}$$

where: V_f : voltage component by f frequency; P_f : psophometric weigh by f frequency; $P_{800} = 1000$.

The psophometric weight has been determined after human tests; it could be seen on Fig. 1. It could be concluded that the main part of the noise disturbance is caused by the 800 Hz and surrounding harmonics. The psophometric weighting could be applied for the current components, too, the formula is the same like in (3), however, this value is characteristic to the zero sequence current of power line regarding its possible disturbing effect. This is the so called disturbing current [1].

1.1.3. Active filtering

Several researchers propose the installation of active filter in order to damp the harmonic resonance effect. The magnitude of damping provided by the active filter, the level of

harmonic distortion, may become worse in certain locations along the radial line. One solution is to use multiple active filters located in the proximity of nonlinear load element. In case of railway transportation, the power system pollution is mainly originated by the use of DC locomotives equipped with rectifier units (fig. 2).

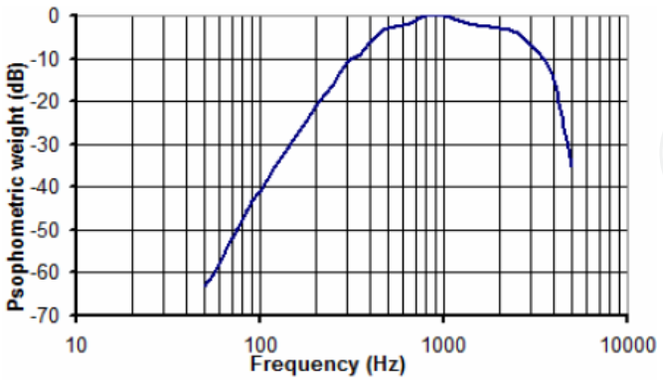

Figure 1. The psophometric weight

The harmonic filters are mandatory to limit the harmonic currents flowing into upstream network and to decrease the resonance effect causing current amplification along the 25 kV supply line. The combination of power factor correction capacitors, parasitic capacitance of contact line and the system inductance (power cables, transformers, etc.) often result in resonant frequency in the 600 – 800 Hz range.

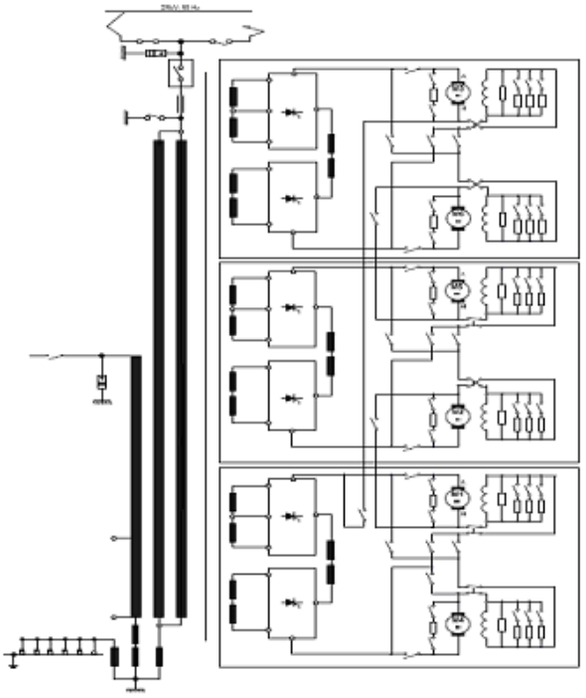

Figure 2. Electrical diagram of the EA – 060 locomotive used in Romania

Most active filter technologies, which focus on compensating harmonic current of nonlinear loads, can not adequately address this issue.

We propose the application of active filters in order to limit the harmonic currents produced by the traction system. The active filter could be located in locomotive or on the substation, or both. Coordination of harmonic of multiple filter units may become a problem since the railway transportation system is characterized by the presence of different types of locomotive from different ages of technology (DC motor with rectifier unit, thyristor). However, in differently from the type of locomotive, the harmonic production needs to be eliminated or limited to a acceptable value imposed by international standards.

In [2] a solution for the coordination of multiple active filters is proposed. The active filter units which are placed on different locations can perform the harmonic filtering without a direct communication using the droop characteristic. We implement the same solution using a fuzzy logic control system.

1.2. Power quality in railway transportation

Power distribution system in electric railway transportation is presented in fig. 3.

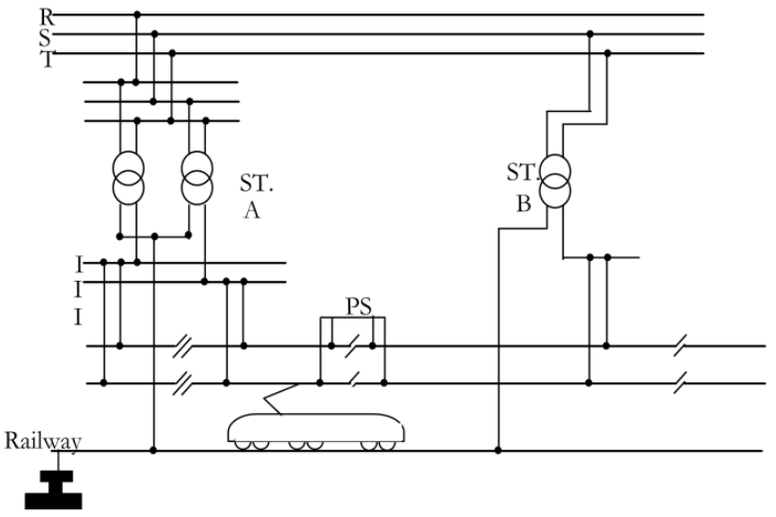

Figure 3. Power distribution system

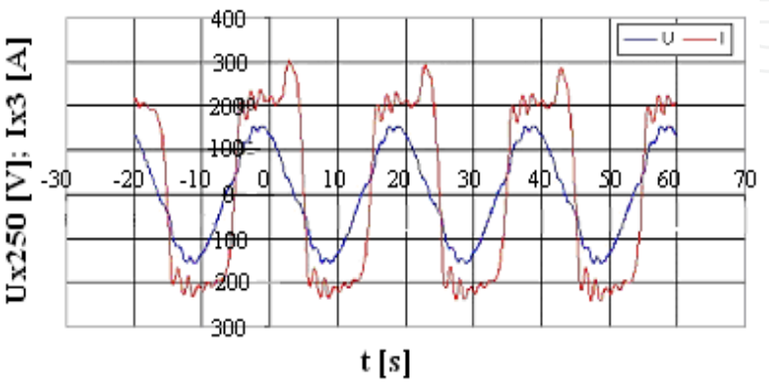

Figure 4. ST load current and voltage waveform in power substation

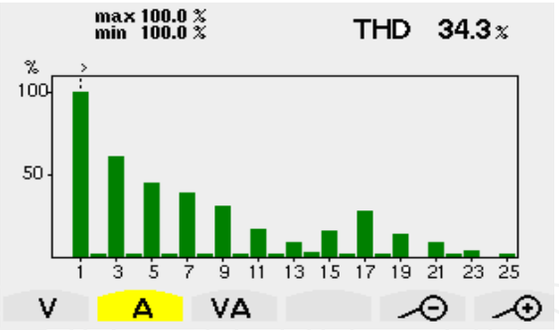

Figure 5. Harmonic spectrum of load current in power substation

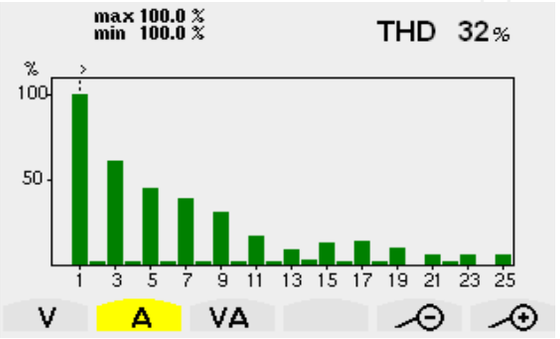

Figure 6. Harmonic spectrum of load current in locomotive

In fig. 4, we present the waveforms for a work regime recorded in a real substation. In fig.s 5 and 6, is presented the harmonic spectrum for the load current in power substation and in locomotive. Comparing these two different spectrums, it could be concluded that the resonance effect is the highest at the 15th and 17th harmonics. Over the 25th harmonics the supply system is decreasing the harmonic current. THD becomes to 34%, far exceeding the admissible values. The resonance phenomenon increase psophometric interference.

1.3. Active filtering solutions for railway power systems

For harmonic compensations in case of railway applications the best choice is the single phase bridge inverter with PWM controlled current control. In order to perform the harmonic compensations it is necessary to present the control structure of the active power filter. The control method is based on instantaneous power theory [3], [4] and [5].

The single phase power system can be defined using:

$$u(t) = U\cos(\omega t) \qquad i(t) = I\cos(\omega t - \varphi) \tag{4}$$

In order to perform the orthogonal transformation of the single phase system to a synchronous reference frame a fictitious imaginary phase defined as is introduced:

$$u_i(t) = U_i\sin(\omega t) \qquad i_i(t) = I_i\sin(\omega t - \varphi) \tag{5}$$

we obtain an orthogonal coordinate system with:

$$u_\alpha = u(t) \text{ and } u_\beta = u_i(t) \tag{6}$$

The active power P_{AV} and Pi_{AV} is given by:

$$P_{AV} = \frac{P_{\alpha\beta AV}}{2} = \left(\frac{2}{T}\right)\int_0^{\frac{T}{4}}\left[u_\alpha i_\alpha + u_\beta i_\beta\right]dt \tag{7}$$

$$P_{i_{AV}} = \frac{P_{i_{\alpha\beta AV}}}{2} = \left(\frac{2}{T}\right)\int_0^{\frac{T}{4}}\left[u_\alpha i_\alpha + u_\beta i_\beta\right]dt \tag{8}$$

The instantaneous power is:

$$\begin{aligned} p_{\alpha\beta} &= u_\alpha i_\alpha + u_\beta i_\beta \quad (a) \\ q_{\alpha\beta} &= u_\alpha i_\alpha - u_\beta i_\beta \quad (b) \end{aligned} \tag{9}$$

And the power factor is given by:

$$\varphi = arctg\left(\frac{q_{\alpha\beta}}{p_{\alpha\beta}}\right) \tag{10}$$

Using p-q-r power theory introduced by Kim and Akagi, allows to present the power situation in synchronous rotation frame. In case we have:

$$u_{\alpha\beta} = \sqrt{{u_\alpha}^2 + {u_\beta}^2} \tag{11}$$

and

$$\theta = \tan^{-1}\left(\frac{u_\beta}{u_\alpha}\right) \tag{12}$$

$$\begin{bmatrix} u_p \\ u_q \\ u_r \end{bmatrix} = \frac{1}{u_{\alpha\beta}}\begin{bmatrix} u_\alpha & u_\beta & 0 \\ 0 & 0 & 0 \\ 0 & 0 & u_{\alpha\beta} \end{bmatrix}\begin{bmatrix} u_\alpha \\ u_\beta \\ 0 \end{bmatrix} = \begin{bmatrix} u_{\alpha\beta} \\ 0 \\ 0 \end{bmatrix} \tag{13}$$

and similarly

$$\begin{bmatrix} i_p \\ i_q \\ i_r \end{bmatrix} = \frac{1}{u_{\alpha\beta}}\begin{bmatrix} u_\alpha & u_\beta & 0 \\ 0 & 0 & 0 \\ 0 & 0 & u_{\alpha\beta} \end{bmatrix}\begin{bmatrix} i_\alpha \\ i_\beta \\ 0 \end{bmatrix} = \begin{bmatrix} i_{\alpha\beta} \\ 0 \\ 0 \end{bmatrix} \tag{14}$$

where:

$$i_{\alpha\beta} = \frac{p_{\alpha\beta}}{u_{\alpha\beta}} \tag{15}$$

where as:

$$p_{\alpha\beta} = u_\alpha i_\alpha + u_\alpha i_\alpha = p \tag{16}$$

Finally we can state:

$$\begin{aligned} u_p &= u_{\alpha\beta} && (a)\\ i_p &= i_{\alpha\beta} && (b)\\ u_q &= u_r \equiv i_q = i_r = 0 && (c)\\ p &= u_p i_p && (d) \end{aligned} \tag{17}$$

From (9a,b) can be obtain

$$\begin{bmatrix} i_\alpha \\ i_\beta \end{bmatrix} = \frac{1}{u^2{}_{\alpha\beta}} \begin{bmatrix} u_\alpha & -u_\beta \\ u_\beta & u_\alpha \end{bmatrix} \begin{bmatrix} P_{AV} + p_{\sim} \\ Q_{AV} + q_{\sim} \end{bmatrix} \tag{18}$$

In order to realize the compensation of whole reactive and distortion powers is necessary to compensate Q_{AV} – component as well as to filter $q_{\sim}$ and $p_{\sim}$ components. The reference current is:

$$i_{REF} = \frac{1}{u^2{}_{\alpha\beta}} \left[u_\alpha \left(p - P_{AV} \right) - u_\beta \left(Q_{AV} + q_{\sim} \right) \right] \tag{19}$$

In fig. 7 we present the active power filter operation considered in two cases: substation placed AF and locomotive placed AF.

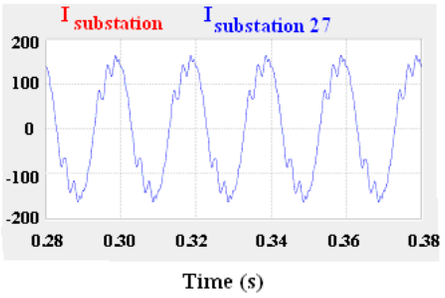

Figure 7. Substation current without filtering at 25 kV and the current in 110 kV network

As it can be observed the placement of active filters in only one place can not provide the necessary filtering in the power line feeding the substation simultaneously to the contact line filtering.

Due to this fact it is necessary to adopt different control strategy and solutions.

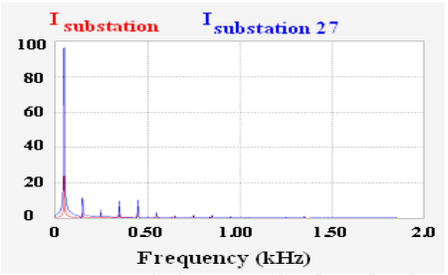

Figure 8. Substation Harmonics without filtering

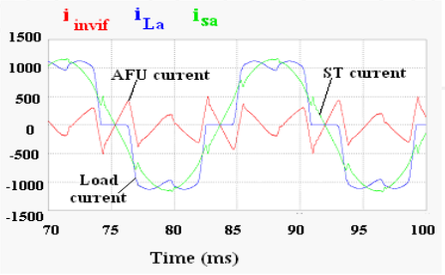

Figure 9. Substation AFU waveforms in substation and in locomotive unit

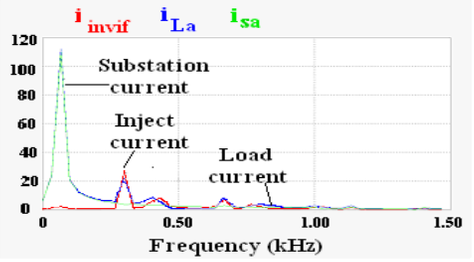

Figure 10. Harmonic components for active filter placed

1.3.1. Coordination of multiple active filters in railway power systems

We propose a solution which has the advantage to share the workload of harmonic filtering between several active filter units. This solution was presented in [2] for the situation of industrial power lines. In our situation we consider the case when the railway system is equipped with active filter unit placed in the substation and locomotive has also an active filter unit integrated. In this case using the existing control algorithms, the harmonic filtering is not coordinated between the locomotive and substation because this would required a real time communication between the AF unit of the locomotive and AF in the substation. This impossible task can be performed using the distributed active filter solution presented in [2] which has been proved to be valid in industrial power systems equipped with distributed active filters (DAFS).

Using this method, several active filter units are installed along the electric power line. All the active filter units operate as a harmonic conductance to reduce voltage harmonics. The active filter unit acts as given:

$$i_x = G_x \cdot U_{x,h} \tag{20}$$

where $U_{x,h}$ represents the harmonic components of the line voltage U_x.

The line voltage U_x is measured and transformed into U_{xq}^{e} and U_{xd}^{e} using high pass filters (HPF), the ripples of U_{xq}^{e} and U_{xd}^{e} are extracted. The voltage harmonics U_{xq}^{e} and U_{xd}^{e} are then multiplied by the conductance command of the active filter. Based on the current command and the measured current, the current regulator calculate the voltage command

$$v_x^* = \frac{L_x}{\Delta T}\left(i_x^* - i_x\right) + U_x \tag{21}$$

In order to share the harmonic workload among the active filter units, it is necessary to use the droop relationship between the conductance command and the volt-ampere of the active filter unit.

$$G_x = G_{x0} + b_x(S_x - S_{x0}) \tag{22}$$

where: G_x are the conductance command for the active filter units; G_0 and S_0 are the rated operation point of each active filter unit.

The conductance command G_x of active filter unit (AFU_x) is determinate by the volt-ampere consumption of this active filter unit. To obtain the volt-ampere S_x of AFU_x, the RMS values of voltage and current associated with AFU_x are calculated:

$$\begin{aligned} U_{xRMS} &= \sqrt{\left\{\left(U_{xq}^{s}\right)^2 + \left(U_{xd}^{s}\right)^2\right\}dc} \\ i_{xRMS} &= \sqrt{\left\{\left(i_{xq}^{s}\right)^2 + \left(i_{xd}^{s}\right)^2\right\}dc} \\ S_x &= U_{xRMS} \cdot i_{xRMS} \end{aligned} \tag{23}$$

where the dc values are extracted by low-pass filters. E_x is the stationary frame value of the current i_x. We consider the case of coordination between the substation active filter AFUx and railway locomotive filter AFU_y. The volt-ampere associated with AFUx and AFU_y can be expressed as following:

$$\begin{aligned} S_x &= \left|U_x\right| \cdot G_x \left|U_{x,h}\right| \approx \left|U_{x,f}\right| \cdot G_x \left|U_{x,h}\right| \\ S_y &= \left|U_y\right| \cdot G_y \left|U_{y,h}\right| \approx \left|U_{y,f}\right| \cdot G_y \left|U_{y,h}\right| \end{aligned} \tag{24}$$

The droop characteristics of both active filter units are given:

$$\begin{aligned} G_x &= G_{x0} + b_x(S_x - S_{x0}) \\ G_y &= G_{y0} + b_y(S_y - S_{y0}) \end{aligned} \tag{25}$$

Based on (24) and (25), the relationship between S_x and B_x can be derived:

$$S_x = \frac{b_x S_{x0} - G_{x0}}{b_x} \quad S_y = \frac{b_y S_{y0} - G_{y0}}{b_y} \tag{26}$$

If the droop characteristics of the active filter units are assigned as follows:

$$G_{x0} - b_x S_{x0} = G_{y0} - b_y S_{y0} \tag{27}$$

$$b_x S_x \approx b_y S_y \tag{28}$$

The slope of the droop should be set in inverse-proportion to the volt-ampere rating of each AFU_s to achieve the desired load distribution. This can be extended to the case of multiple installations of active filter units.

$$b_x S_{x0} = b_y S_{y0} \tag{29}$$

The above droop settings allow harmonic filtering workload being shared in proportion to the volt-ampere rating of the active filter units. The control structure of the proposed system is presented in fig. 11. In our case since the system has a rather variable structure (due to the traffic variability and locomotive distribution) we propose a fuzzy logic conductance calculator.

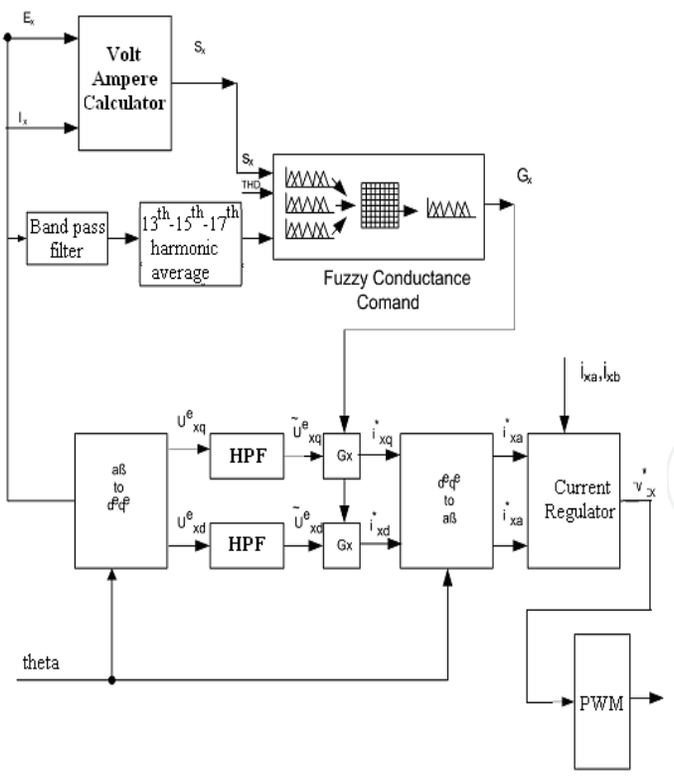

Figure 11. Fuzzy logic control for the active filter distribution

This calculator identifies the appropriate value of the Gx according to the actual load and load capability of the filter and the harmonic spectrum characteristic. Considering the case

when the active filter AF1 is located in substation and we have also an active filter operating at locomotive level we can coordinate them using a load sharing algorithm which is implemented by the fuzzy logic conductance command block.

The phase line voltage is measured and transformed into Uxq and Uxd in synchronous reference frame. Using high pass filters (HPF), the voltage line harmonics are extracted and multiplied by the conductance command Gx computed by the fuzzy logic conductance controller. The current commands Ixs and Ixd of the active filter computed by the Clark transformation block are transformed to the current commands I_x. Based on the current command, the current regulator calculates the voltage command Vx as given:

$$v_x^* = \frac{L_x}{\Delta T}(i_x^* - i_x) + U_x \tag{30}$$

The fuzzy logic command can be tuned according to the capability of each unit in order to have a different response for each situation.

The principle of operation of the fuzzy logic conductance command block is based on the analysis of three parameters : the volt ampere S_x for the corresponding active filter, the total THD of the current measured in active filter location and the averaged value of the sensitive harmonics (in our case the 13^{th}-17^{th} harmonic).

1.4. Fuzzy logic conductance command block

The fuzzy logic conductance block is designed in order to reduce the harmonic distortion components considering the distribution of the active filters. The distortion components bare reduced using the fuzzy inference, the fuzzy logic conductance reacts differently in function of filter volt-ampere, THD value and in order to avoid resonance, the average value of 15^{th}-17^{th}-19^{th} harmonics.

The variables of the inference system were represented as membership functions and the normalization of the each input variable was made in order to match the value of the inputs $0 \div 1$ range.

In fig.s 12, 13 and 14 are presented the membership functions for the input magnitudes, and in fig. 15 is presented the membership functions for the output magnitude.

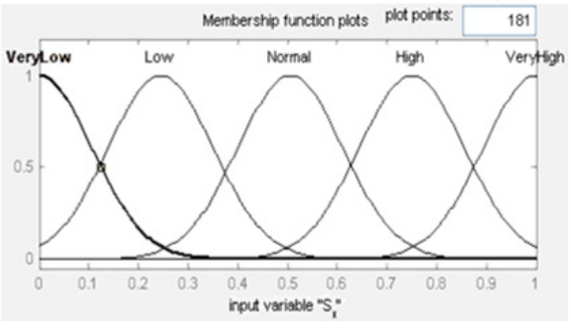

Figure 12. Membership functions for S_x

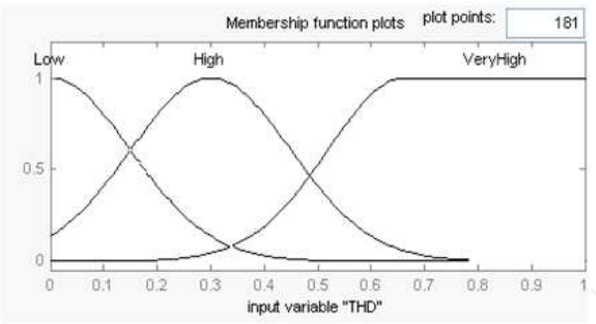

Figure 13. Membership functions for THD

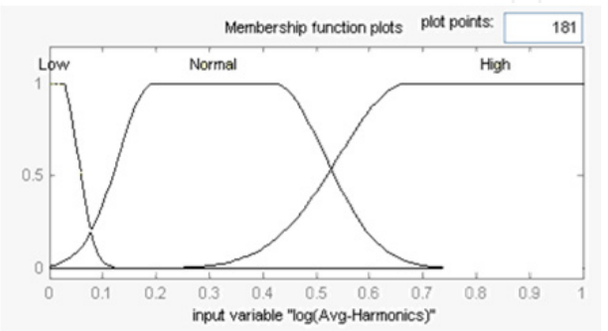

Figure 14. Membership functions for Avg Harmonics

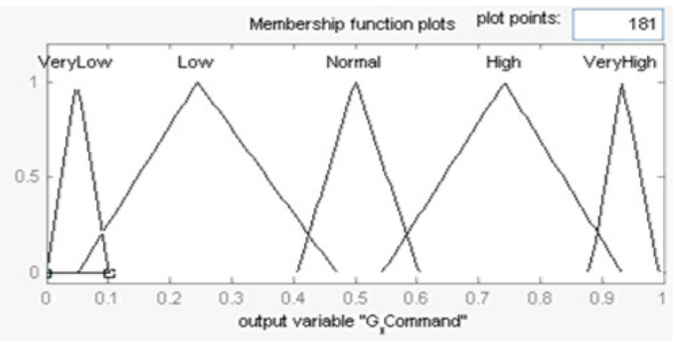

Figure 15. Membership functions for G_x Command

The most important element of the fuzzy systems is the base of rules which implements the relationship between the inputs and the output of the system. The response surfaces of the system are presented in fig.s 16 and 17.

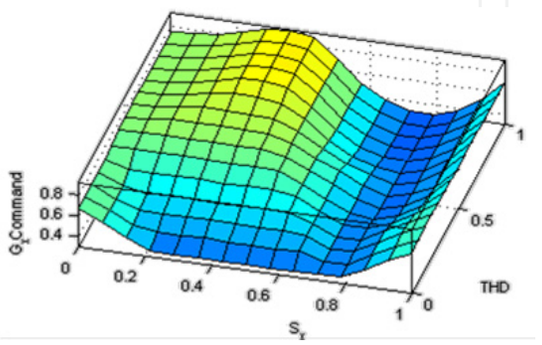

Figure 16. Surface G_x vs. THD and S_x

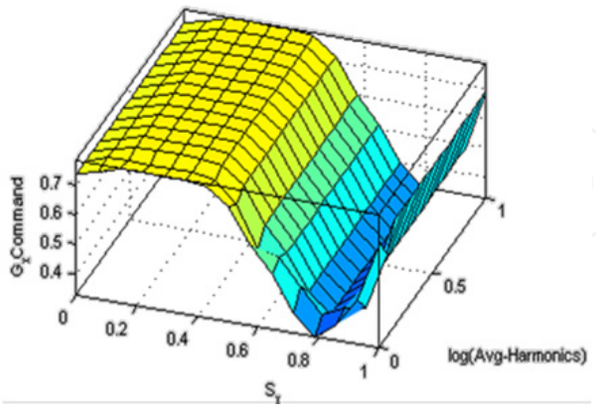

Figure 17. Surface G_x vs. THD and log(Avg-Harmonic)

1.5. Simulation results

The control algorithm is implemented in PSIM and the control in Matlab Simulink and fuzzy logic toolbox (fig. 18). The proposed solution is applied for the railway power distribution system in order to demonstrate its capability to share the harmonic filter among the various active filter units.

The current and voltage component on the filtered harmonic orders are reduced dramatically and the typical effect of the 3rd and 5th harmonics have been neglected, but the significant high frequency components (mainly 17th and 19th harmonics).

The circuit model of the railway is illustrated in fig. 19. Two active filter units are placed, one in substation location and the 2nd at the locomotive level. The locomotive represents a nonlinear load comprising several rectifier units. The parameters of the simulation are given as follows: power system (27kV, 50Hz); line parameters usual values in railway transportation 0,47Ω/km.

The control structure is similar for each unit but the filters characteristics need to be tuned according to their location.

Fig. 9 contains the wave forms when both active filter are working. The harmonic distortion is improved as the THD are reduce by the filter in action of the AF_1 and AF_2.

The active filter units of the DAFS adjust the conductance command G_1 and G_2 based on their own droop characteristics for the volt-ampere consumption for AF_1 and AF_2, which indicates that the filtering workload is evenly shared between the active filter units of the system (fig. 20 and 21).

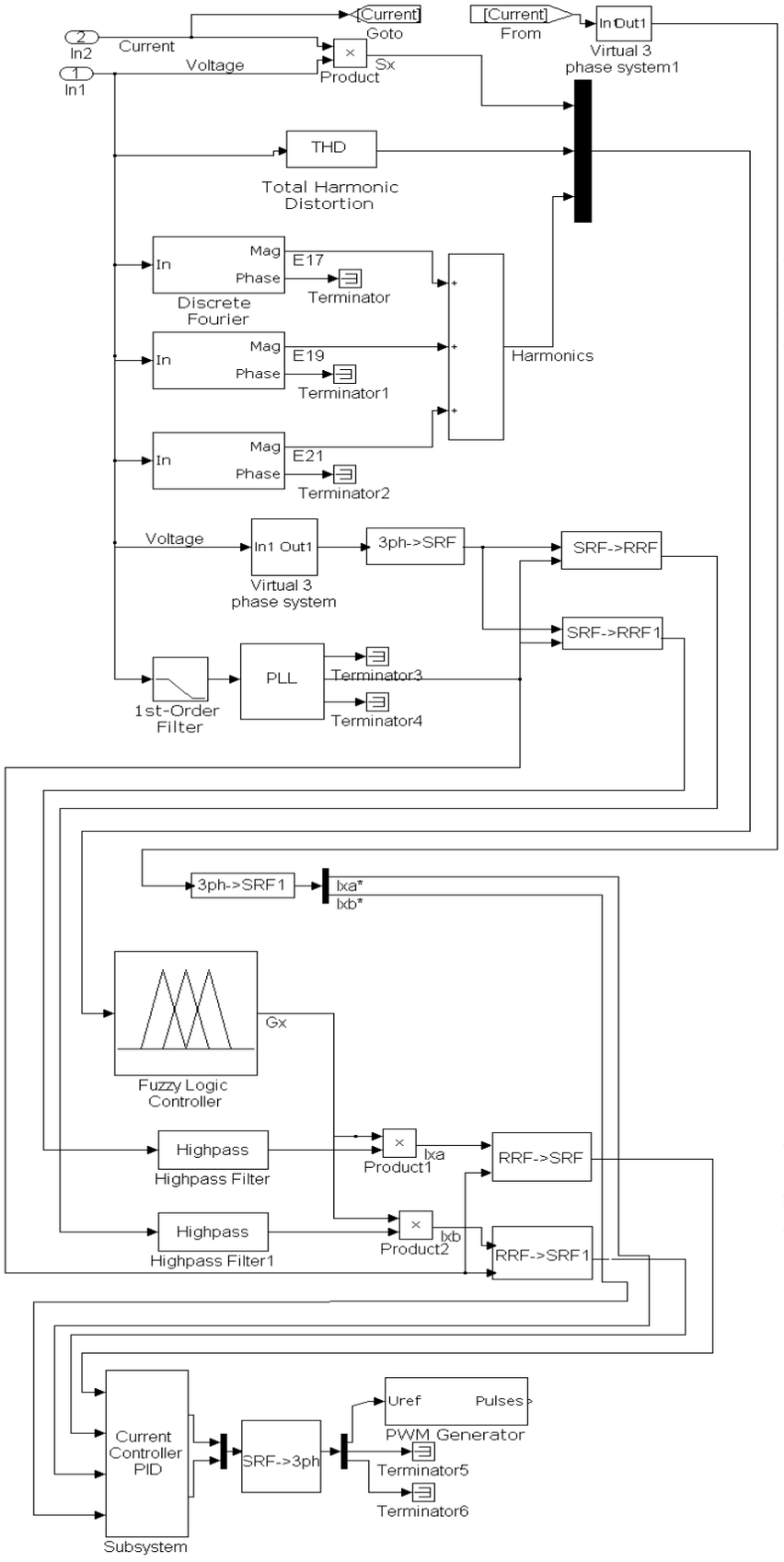

Figure 18. Fuzzy logic control for the distributed active filter

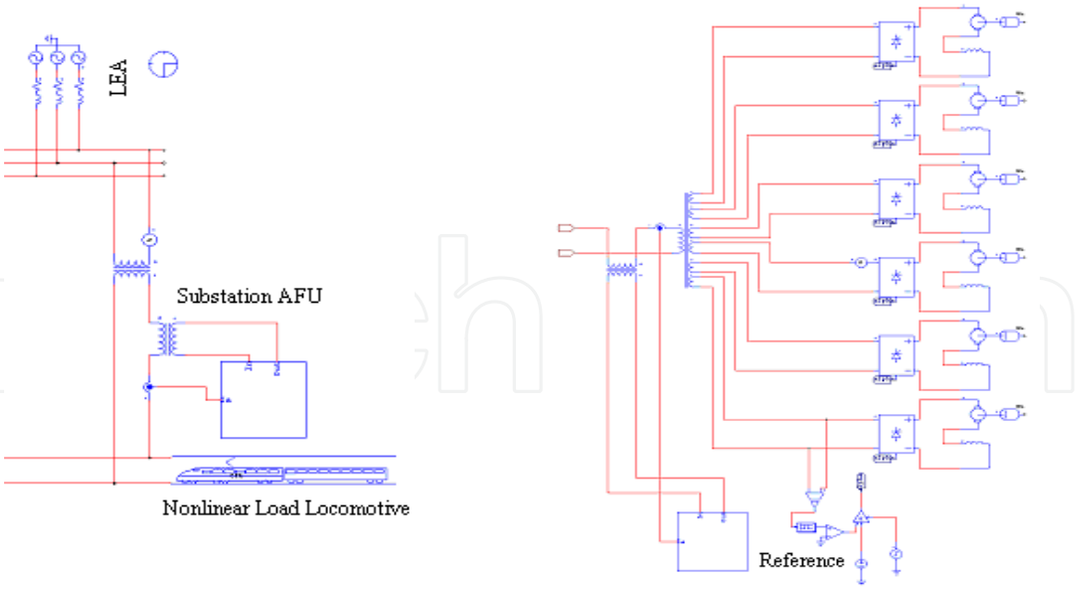

(a) Substation model (b) Locomotive model

Figure 19. a) and b). Railway power system simulation

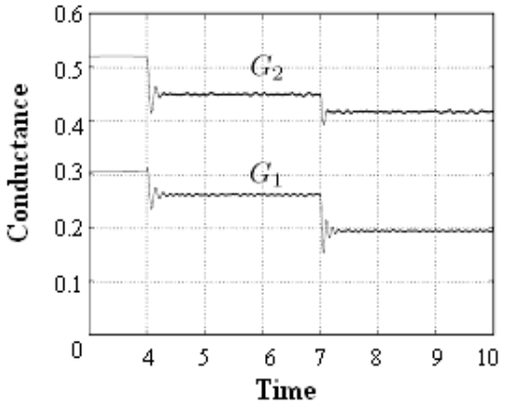

Figure 20. Variation of G_1 and G_2.

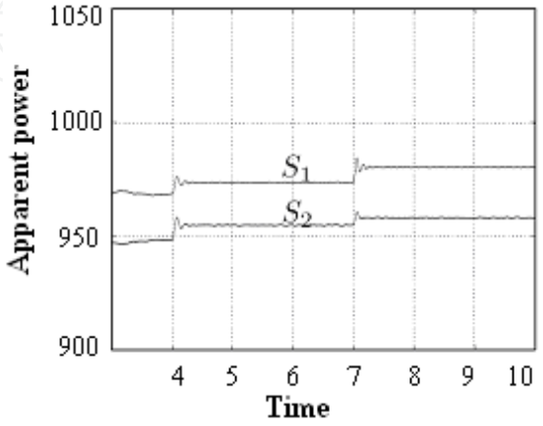

Figure 21. Variation of S_1 and S_2

2. B. Advanced system for the control of work regime of railway electric drive equipment

2.1. Introduction

Although the contact line in electric railway transport (and not only) can be regarded as a line of electric power distribution, it has several (mechanical and electric) characteristics that differ from the usual power systems. Thus, the most common failure regimes are the short circuit in the contact line (L.C.), sub-sectioning (P.S.) or in traction sub-stations (ST), produced by dielectric breakdown of insulators or mechanical failures caused by the pantograph of the electric engine (fig. 22).

The sudden growth of currents in the case of short circuits has negative consequences both upon the fixed installations of electric traction (thermal and dynamic effects) and upon other nearby installations (dangerous inductions in the phone networks, in the low voltage grids on pipelines, etc., which can endanger the life of the personnel in the vicinity of the railways.

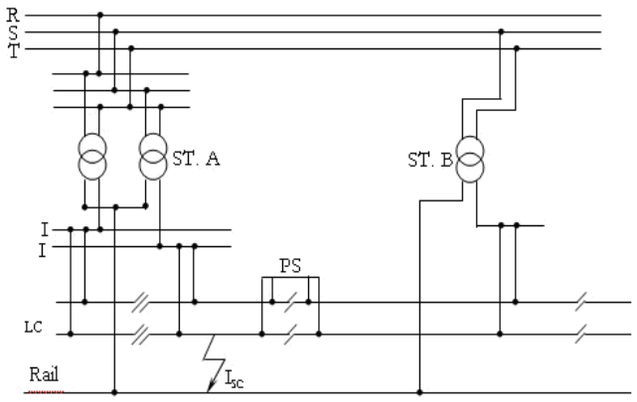

Figure 22. Electric power feeding of railway traction

In the case of single-phase electric railways with the frequency of 50 Hz, the distance between two ST is 50 ÷ 60 km, depending on the profile of the line. For the simple lines, the high value of characteristic impedance (0,47 Ω/km), leads to minimal short circuit currents (at the end of the line), below the maximal load currents.

In the case of short circuits in the vicinity of the ST, the currents reach up to eight times the charge current, and this is why they have to be cut off as quickly as possible. Neither the low current short circuits must be maintained for too long, as they have negative effects upon the installation.

Because of the elements mentioned above, protecting the contact line feeders by maximal current protection is not efficient enough. At present, distance protection is being used, either by di/dt relays or by impedance ones.

The di/dt relays function on the basis of the existing deforming regime existing in the contact line, current regime which should be diminished as much as possible in the future. The elimination of the deforming regime will make the di/dt relay inefficient.

Impedance relays, which are widely used in all power systems, can distinguish between an overload and a short circuit [11]. Because of the configuration of the contact line, the shape of the RX characteristic of the relay in the complex plane should be modified for each traction substation separately, which is difficult to achieve in practice. In order that RX characteristic meets the requirements imposed to the protection system, the complexity and cost increase [12].

2.2. The structure of the protection device

In order to secure protection against the abnormal work regimes of the contact lines and transformers, we designed a complex device meant to replace both the maximal current, low voltage relays etc., and the impedance relay. The block diagram of the device is given in fig. 23 [10].

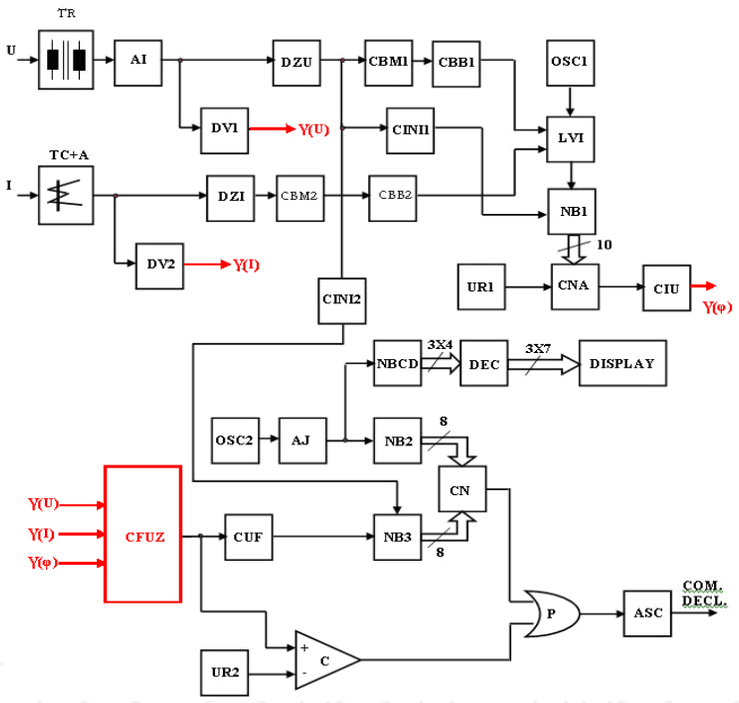

Figure 23. The block diagram of the protection device

The voltage of the power circuit is converted to a reduced value, accepted by the electronic circuit, by means of a group of instrument transformers TR, thus achieving, at the same time, galvanic separation of the power circuit using the insulation amplifier AI, which works with unitary amplification factor. At the output of the insulation amplifier AI we obtained an alternating voltage with a maximal amplitude of 10 V, fed both to a peak detector DV1 and to a device meant to detect the passage through zero of the voltage wave, DZU .

At the output of the peak detector DV1 we obtained signal V(U), whose value is proportional to the value of the voltage in the power circuit. Signal V(U) is fed to one of the analogue inputs of the fuzzy microcontroller. The voltage wave zero passage detector,

marked DZU, is meant to generate an impulse at each such passage. The impulse obtained at the output of this block is fed on the one hand to a monostable switch circuit CBM1, in order to obtain a square impulse with a well determined shape and duration, and on the other hand, to an initialization circuit, CINI1. The signal at the output of the monostable switch circuit CBM1 is fed to the bistable switch circuit CBB1, triggering the switch of its output at each impulse received. The bistable switch circuit CBB1 is meant to trigger the determination the phase shift between the voltage and the current in the power circuit by means of a validation/inhibition logic (block LVI) of the access of some square impulses generated by the oscillator OSC 1 and fed to the asynchronous binary counter NB1.

The value of the current in the power circuit is converted by the ensemble current translator – amplifier TC+A into a voltage signal V(I) whose amplitude is 10V, which is fed to the peak detector DV2. At the output of the peak detector we obtain signal V(I), which is fed to one of the analogue inputs of the fuzzy controller. The current signal is also fed to a zero passage detector of the signal corresponding to the current, DZI, which commands a monostable switch circuit, CBM2, and a bistable switch circuit CBB2, both having similar functions with those on the branch corresponding to the voltage wave. The bistable switch circuit CBB2 is meant to stop the phase shift determination process, and it acts in this sense through the validation/inhibition logic.

As shown before, we input to the fuzzy microcontroller three analogue signals V(U), V(I) and V(ϕ), having values ranging between (0…5) V, whose values depend on the voltage, current and phase shift in the power grid. According to the value of the three signals and using the original processing program implemented on the fuzzy controller under the form of processing rules, at its analogue output we obtained a continuous voltage ranging in the domain (0…5)V. Its value is higher when the regime on the contact line approaches the failure regime, respectively when it is under failure regime and it is directly proportional to the seriousness of the failure.

What has to be done is to disconnect the contact line in a time interval that is inversely proportional to the seriousness of the failure. At the same time, it is necessary to keep on feeding the contact line in the situation of short term failures (caused for instance by atmospheric overcharges).

Meeting these requirements can be achieved by a programmable time delay circuit. This is made of a voltage – frequency converter connected to the output of the fuzzy controller, where a square signal is obtained, whose frequency is directly proportional to the voltage given by the fuzzy controller. These square impulses are then fed to a binary counter NB3, which shows – during one counting period – a value which is directly proportional to the voltage at the output of the fuzzy microcontroller. Counter NB3 is set on 8 binary ranks. Its outputs are fed to the input of a numeric comparator , CN. At the other inputs of the numeric comparator we apply the outputs of another binary comparator NB2, that is meant to memorize a value pre-established by the user. This value is input to the counter by means of the adjusting block AJ, respectively of the tact oscillator OSC2. The impulses fed to binary counter NB2 are simultaneously fed to a decimal code counter NBCD, whose outputs are

connected to a decoding system DEC and then to a 7-segment display, marked DISPLAY. In this way, the user has a permanent control over the value given by binary counter NB2. This value represents the very threshold that triggers the main contact line feeding interrupter. Numeric comparator CN signals the situation when the numeric value in counter NB3 becomes equal to the threshold value in counter NB2. It is necessary to enable the modification of the threshold value for the main interrupter, according to the various normal functioning regimes established by the concrete practical situation and which have to be dealt with accordingly. The threshold is established by the users, according to the experience accumulated in time.

It is obvious that the triggering of the contact line main feeding interrupter is done in a time interval that is directly proportional to the threshold value in binary counter NB2, and inversely proportional to the voltage at the analogue output of the fuzzy microcontroller. The main interrupter can be triggered almost instantaneously, if the fuzzy microcontroller outputs a 5V voltage, which corresponds to highly dangerous failure. This value is sensed by comparator C, which permanently compares the output value of the fuzzy controller to a 5V reference voltage, fed by reference source UR2.

In case of reaching a regime that triggers the main interrupter, at the output of port P we have logic 1. This signal is power amplified by means of command signal amplifier ASC, which outputs a high enough signal to command the main interrupter.

For a correct functioning, binary counter NB3 has to be periodically reset, so that its value should not reach the threshold value memorized by binary counter NB2, even under a normal functioning regime. This condition is met during each period of the voltage in the grid, by initialization circuit CINI2. This circuit too, uses as time reference the zero passage impulse of the grid voltage. It is preferable to initialize counter NB3 just once during one period, as in this case, the value of counter NB3 depends on two operations of phase determination – corresponding to the two semiperiods – which achieves in this way a high immunity to very short perturbations or incorrect work regimes along the contact line.

All the circuits presented above have been designed built and tested and they worked correctly.

2.3. The Fuzzy Controller

As mentioned before, in order to offer a complex protection of the contact line in railway electric transport, using mono-phase AC (27,5 [kV], 50 [Hz]) we designed a Fuzzy relay, starting from the practical case of a railway electric traction sub-station [10]. This relay allows a maximal current, overcharge, distance and minimal voltage protection. Although initially we did not take into consideration directional protection (the inverse current circulation between two traction substations), its introduction is not a problem and we consider that the Fuzzy relay can achieve that too.

a. Information on the input magnitudes

We considered the following usual regimes:

Variable		Linguistic values	Variation domain	Universe of discourse [%]
Input	Current	normal	50 ÷ 600 [A]	0÷30,8
		overcharge	600÷800 [A]	25,6÷41
		short-circuit	800÷2000 [A]	35,9÷100
	Voltage	short-circuit	16 ÷ 20 [kV]	0÷43,5
		overcharge	20 ÷ 25 [kV]	26,1÷87
		normal	25 ÷ 27,5 [kV]	69,6÷100
	Phase shift	normal	0÷30 [grad]	0÷43,8
		overcharge	30÷60 [grad]	31,3÷81,3
		short-circuit	60÷80 [grad]	68,8÷100
Output	Command	blocked	0 [V]	0
		high delay	1,66 [V]	33,3
		low delay	3,33 [V]	66,6
		instant	5 [V]	100

Table 1. Input and Output Magnitudes

In figure 24 we present the recorded values for the current in one ST with high traffic protected with usual distance relay. One may notice a rather high frequency of critical work regimes transitory (three short-circuits at long distance, without disconnection due to a mechanical failure: 1, 2, 4; and three overloads: 3, 5 and 6 all in a period of twenty minutes). The waveforms for three cases: normal, overload and short-circuit are presented in figures 25, 26 and 27. The phase shift between current and voltage for three situations are clearly different which justify the selection of phase as an important factor in identification of critical regimes. Another interesting characteristic is the smoothing of the current waveform during the short-circuit situation (even in the case of long distance short-circuit) and the phase shift increase which is produced by the change of the complex impedance of the system.

As the scale representing the transfer functions that correspond to the processed magnitudes is a percentage one (0 - 100%), we needed to norm the discussion universe, by means of a 1st degree polynomial function.

In fig. 28, 29, 30 are presented the membership functions for the input magnitudes, and in fig. 31 is present the output magnitude.

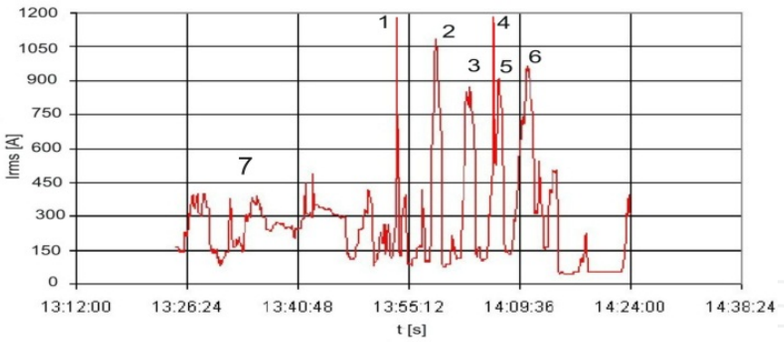

Figure 24. ST load current in different work conditions: 1,2,4 – long distance short-circuit; 3,5,6 – overload; 7 – normal load

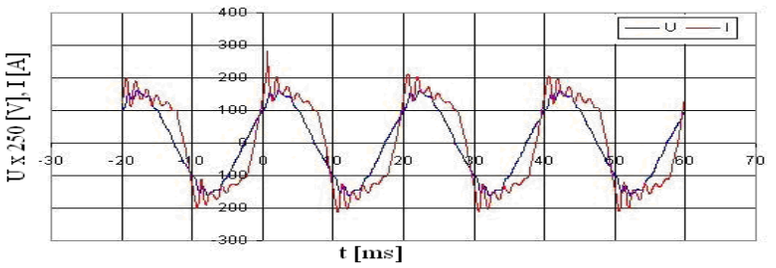

Figure 25. ST load current and voltage wave in normal regime

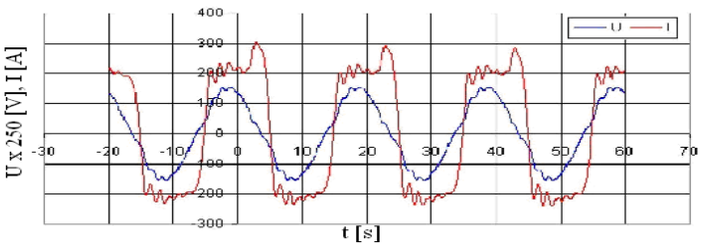

Figure 26. ST load current and voltage wave form in overload regime

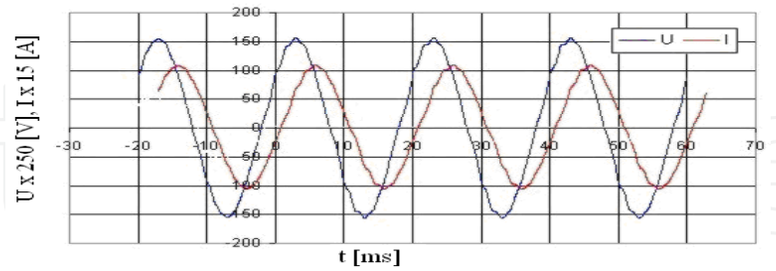

Figure 27. ST load current and voltage in short-circuit regime

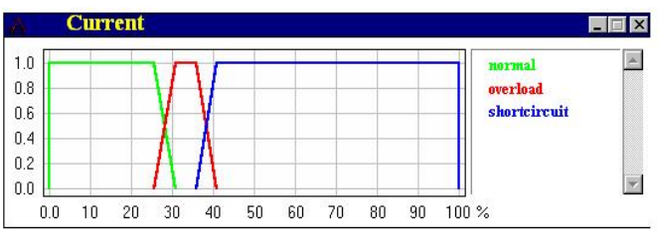

Figure 28. Representation of membership functions for the input magnitude "current"

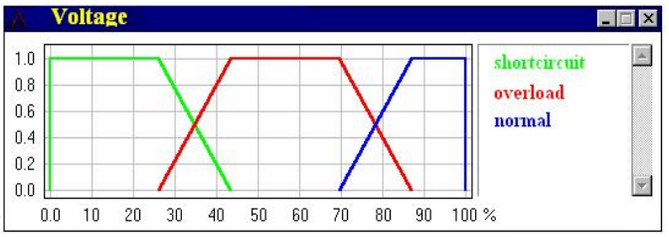

Figure 29. Representation of membership functions for the input magnitude "voltage"

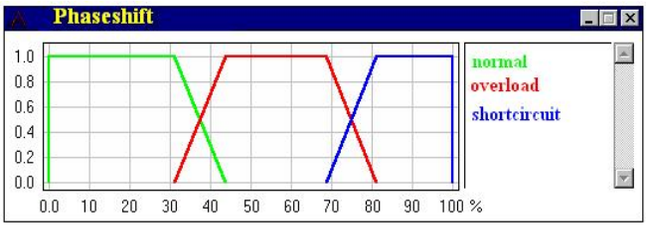

Figure 30. Representation of membership functions for the input magnitude "phase shift"

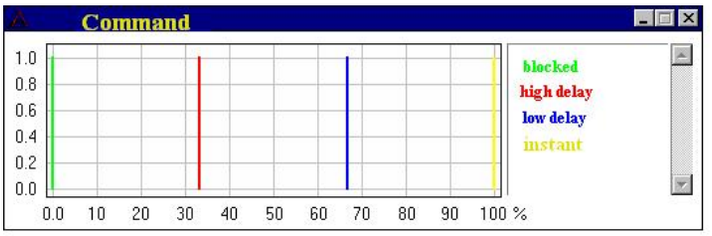

Figure 31. Representation of membership functions for the output magnitude "command"

b. Command rules (inference)

The rules have been established for practical reasons after having checked the reference literature and consulted experts in electric traction and protection installations for electrical systems.

Fig. 32 shows the rules base which connecting the fuzzy input variables to the fuzzy output variable, by means of the inference method (max/min). For deffuzification we chose the Singleton weight centers method due to its major advantage, namely the short processing time, a stringent condition for the real time functioning of the Fuzzy controller with a function of relay. For this reason, for the practical application under analysis we established Singleton-type membership functions corresponding to the linguistic term "command" of the output magnitude. Using the max-min inference method alongside with the defuzzification method is widely spread in practice and has lead to outstanding performances of the regulation systems.

Fig. 33 shows the command surface for three constant values voltage corresponding to the cases described above (normal, overload and short-circuit).

Rule Base Editor

TABLE	If			then	
	current	voltage	phaseshift	command	weight
1. Rule	normal	normal	normal	blocked	1.0
2. Rule	normal	normal	overload	high delay	1.0
3. Rule	normal	normal	short-circuit	instant	1.0
4. Rule	normal	overload	normal	low delay	1.0
5. Rule	normal	overload	overload	high delay	1.0
6. Rule	normal	overload	short-circuit	instant	1.0
7. Rule	normal	short-circuit	normal	instant	1.0
8. Rule	normal	short-circuit	overload	instant	1.0
9. Rule	normal	short-circuit	short-circuit	instant	1.0
10. Rule	overload	normal	normal	blocked	1.0
11. Rule	overload	normal	overload	high delay	1.0
12. Rule	overload	normal	short-circuit	instant	1.0
13. Rule	overload	overload	normal	high delay	1.0
14. Rule	overload	overload	overload	low delay	1.0
15. Rule	overload	overload	short-circuit	instant	1.0
16. Rule	overload	short-circuit	normal	high delay	1.0
17. Rule	overload	short-circuit	overload	instant	1.0
18. Rule	overload	short-circuit	short-circuit	instant	1.0
19. Rule	short-circuit	normal	normal	low delay	1.0
20. Rule	short-circuit	normal	overload	low delay	1.0
21. Rule	short-circuit	normal	short-circuit	instant	1.0
22. Rule	short-circuit	overload	normal	low delay	1.0
23. Rule	short-circuit	overload	overload	instant	1.0
24. Rule	short-circuit	overload	short-circuit	instant	1.0
25. Rule	short-circuit	short-circuit	normal	instant	1.0
26. Rule	short-circuit	short-circuit	overload	instant	1.0
27. Rule	short-circuit	short-circuit	short-circuit	instant	1.0

Figure 32. Rules base

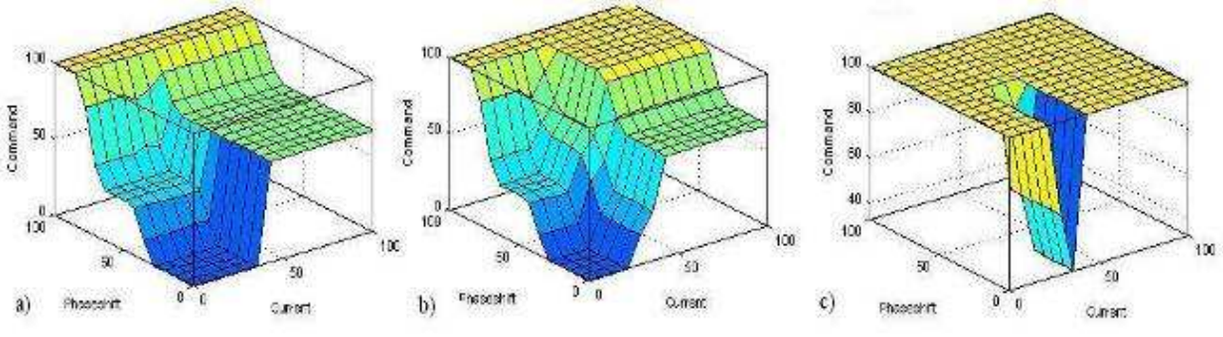

Figure 33. Command surfaces for three voltage values

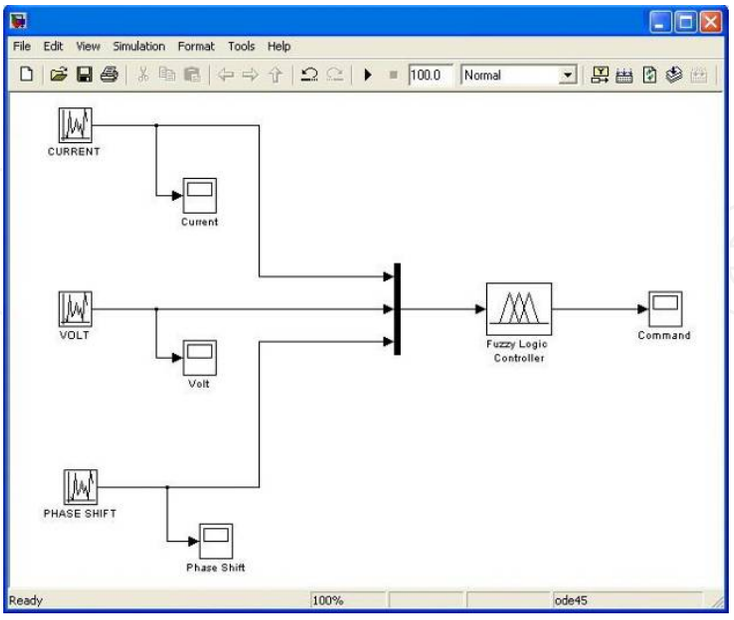

Figure 34. Simulation diagram

Fuzzy controller simulation is realized in Matlab – Simulink (fig. 34). We randomly generated several combinations of input variables (fig. 35, 36 and 37), and the analysis of the response (fig. 38) proved the correct functioning of the fuzzy system, according to the rules base established.

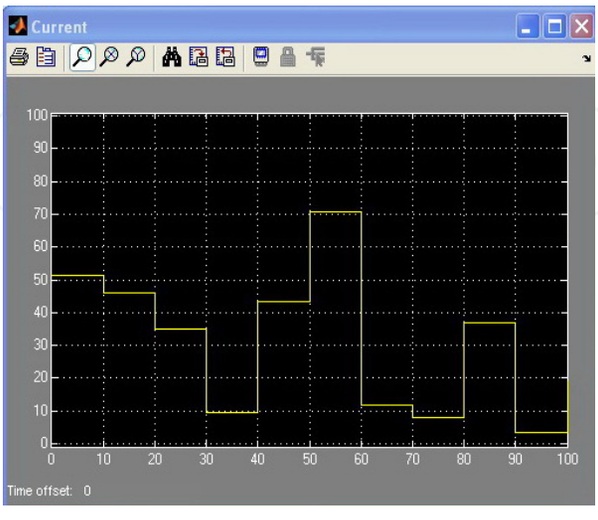

Figure 35. Input magnitude CURRENT

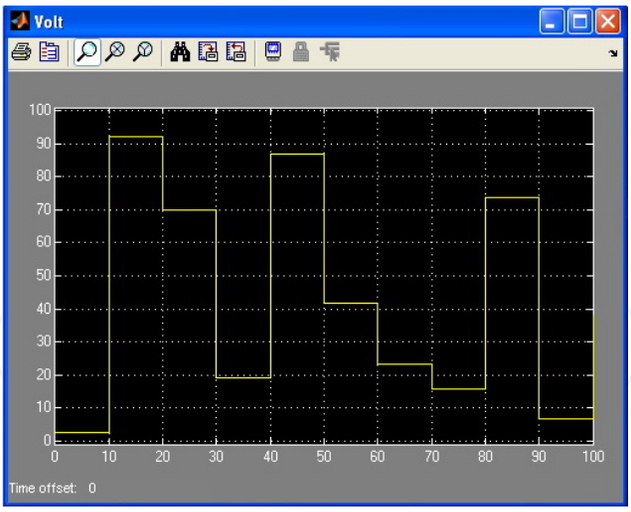

Figure 36. Input magnitude VOLTAGE

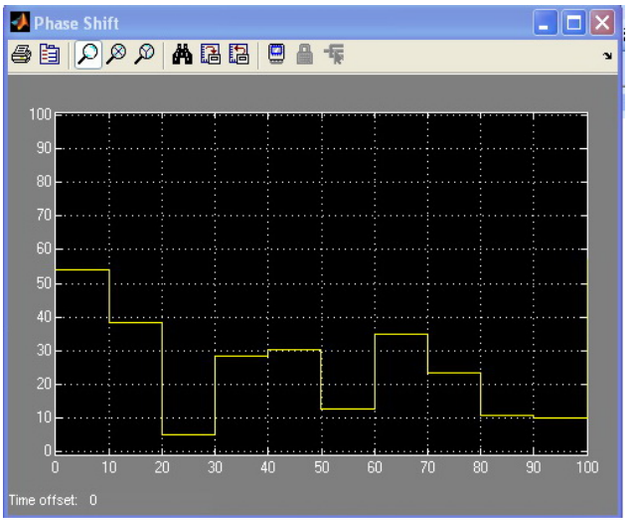

Figure 37. Input magnitude PHASE SHIFT

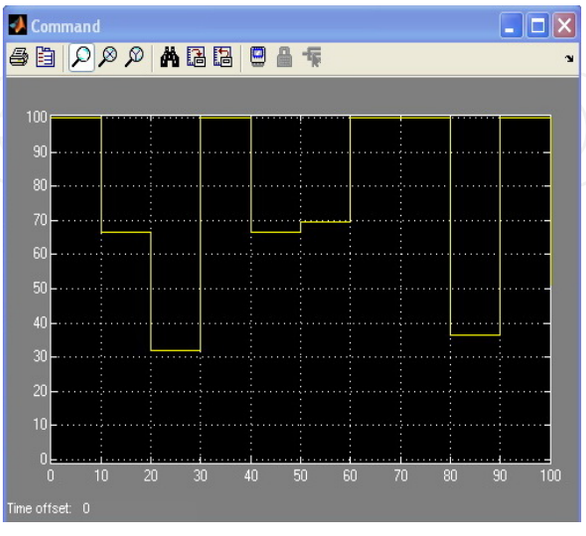

Figure 38. Output magnitude COMMAND

The fuzzy system has been implemented on an eZdsp TMS320F2812 development board produced by Spectrum Digital.

2.4. Hardware implementation and testing for the Fuzzy Logic relay for railway protection

The development cycle is based on three stages: first the fuzzy logic relay is designed and tuned on Matlab – Simulink using a Simpower System model of the railway ST because the testing in the real system would have been extremely expensive and dangerous. This allows the simulation, parameters tuning and optimization of rules data base.

In the second stage, the final structure of the fuzzy logic operations are prepared for hardware implementation. In order to achieve a high speed operation some hardware specific features of the DSP are employed to reduce the computation resources for the application. One operation which requires intensive computation is the deffuzification which need complex instruction. Each input (voltage, current and phase shift) is sampled using an 8 bit ADC. The input variables are quantified in order to obtain the degree of membership of each point of the input for each fuzzy set. For each point is associated an index value corresponding to the membership function. The rule base in coded using the same index system in order to have the correspondence between the index of active membership functions with the corresponding part of the rule base.

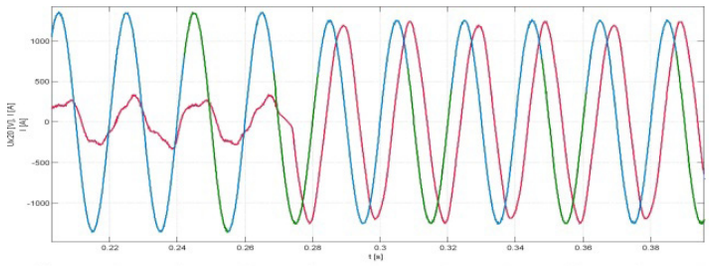

a) long distance short circuit

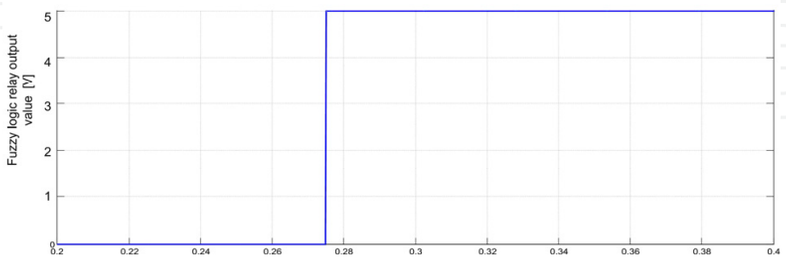

b) relay response

Figure 39. Fault processing by the fuzzy logic relay

Finally, the structure of the system operation is coded using Code Composer Studio development environment in C. The resulting assembly code is optimized for speed in order

to have the shortest cycle time. For the hardware implementation we have considered a Spectrum Digital DSP development board with TMS320F2812 processor.

From the point of computation resources this can offer sufficient processing speed in order to meet the application requirement at a reasonable development time (since no assembly coding was necessary). This hardware solution used to implement the fuzzy logic relay structure is simple and provide good performance/price output.

After manual verification of the correct functioning of the DSP fuzzy processor the entire system was put under test in a real ST (in parallel with the existing protective system). In figure 10 a one long distance short circuit it has been identified and the actual response of the relay is presented in fig 10 b. One may notice the extremely fast response of the proposed fuzzy relay system (the short circuit was not identified by the usual impedance relay due to the misclassification of the fault).

The existing protection system obviously has considered the event as an overload and it disconnected the main switch about one minute after.

3. C. Control system for catenary – Pantograph dynamic interaction force

3.1. Introduction

An issue of great importance in railway electric transportation is the quality of the sliding contact „pantograph- catenary suspension".

An improper contact produces electric arcs with unfavorable consequences on energy loss, reliability and wear of the subassemblies subjected to the arc, electromagnetic pollution, etc.

Of main interest is the behavior of the dynamic response of the two mechanical subsystems coupled by the contact force (pantograph- catenary suspension), each of them having totally different structures and dynamic properties.

The aims of the numerical simulation analysis were to obtain conclusive information for kineto-static and dynamic characterization of the „pantograph - catenary suspension" assembly's behavior.

Based on the simulations performed in this work, using an original program, was found that the dynamic response of the studied assembly produces variation of the contact force in very large ranges, depending on the train's travel speed and other parameters, being the one which leads to detachments, thus to electric arcs.

Currently, there are several world-wide used models for pantograph–catenary interaction, which apply especially at high speeds (over 350km/h) and rely on different principles [19], [20], [21]. These models have different degrees of complexity. Most of them consider simplifications, as taking into account all the factors (i.e. aerodynamic forces, friction, proper oscillation of the locomotive, etc.) leads to a very difficult problem. The traffic at speeds above 350km/h is made on the specific lines, namely the railways, catenary suspensions and locomotives are especially built and designed for these conditions. However, in Romania and the neighboring countries

this traffic runs on normal lines, which through modernization can be improved to support speeds from 140km/h up to 220km/h. In this case the railway, the catenary suspension and the locomotives are just the upgraded classical ones. The current paper refers to this part of this problem, which has not been extensively treated in the literature.

The conclusions presented in this work have a special importance, based on which following to be achieved an intelligent management system of the pantograph's pressure force regime, taking into account the speed, its momentary position and the coupled dynamic model of the two subassemblies: pantograph- catenary suspension.

3.2. Analysis of the "Catenary-Pantograph" assembly's dynamic behavior by numerical simulation

The purpose of the numerical simulation, by results interpretation, was the possibility to test the validity of the issued hypothesis upon the real systems' behavior, being in operation, as *dynamically coupled subassemblies*.

The analysis was made using the *TENSI-CABLE* calculation program, specially conceived by one of this work's authors for the dynamic behavior's study of some strength structures composed by flexible elements.

The program's essence consists in the possibility to determine the structure's response to a dynamic stimulus, of „excitation force" or „imposed motion" type, into a section required by the user. From space and paternity considerate of the calculation program, in this work are presented and commented only the results of some of the performed simulations.

The study of the „catenary suspension–pantograph" assembly's dynamic behavior, conducted by numerical simulation, was made considering a catenary suspension with standard configuration in Romania, having the parameters written in table 2.

Material: Contact wire Carrier cable Articulated pendulum	- copper, section 100 mm^2 - galvanized steel, section 70mm^2 - galvanized wire, section 28 mm^2
Suspension's total length	- 196 m
Distance between the supporting pillars	- 3 spans of 60,0m each
Distance between the articulated pendulums	- 6 m / 8m (9 pendulums per span)
Mechanical stress: Upper wire Lower wire	 - 12.000N - 12.000N
Specific mass: Upper wire Lower wire	 - 0,89 kg/m - 0,61 kg/m
Axial rigidity Upper wire Lower wire	- 10500 kN - 5000 kN

Table 2. Standard's catenary parameters

The catenary simulated is a simple style catenary, which was chosen because it has all the characteristic dynamic effects. A diagram of the model is given in fig. 40, where:

Tower stiffness: S; Dropper stiffness: K; Distance to the i-th tower: W_j; Distance to the i-th dropper: X_j; Stiffness of the two wires: EI_A; EI_B; Density of the two wires: ρ_A; ρ_B; Tension in the two wires: T_A; T_B.

The contact force, as excitation force considered in simulation, is the one afferent to a basic pantograph of which designing parameters are typical to EP3 pantographs, being in current operation at Romanian Railways, (fig. 40).

For the study made on the simulation model, it was built the input data block comprising the determinant geometrical and mechanical parameters for the component elements of the studied assembly.

In simulation were considered three spans of catenary (fig. 41), having a number of 70 nodes and 103 elements.

The equations governing the response of the catenary are obtained through the displacement of the contact wire and messenger wire, expressed as Fourier sine series expansions. The displacement shapes of the contact wire and messenger wire from equilibrium are each expressed as Fourier sine series expansions, and a good approximation of the shape is possible if enough terms are used the series expansions are given below:

$$y_A(x,t) = \sum A_m(t) \sin\left(\frac{m\pi x}{L}\right) \text{- messenger wire} \tag{31}$$

$$y_B(x,t) = \sum B_m(t) \sin\left(\frac{m\pi x}{L}\right) \text{ - contact wire} \tag{32}$$

where: y – the wire displacement; A_m – the amplitude of the m-th sine term for the messenger wire; B_m - the amplitude of the m-th sine term for the contact wire; x – the displacement along the catenary; L – the total length of the catenary; m – an integer, designates the harmonic number.

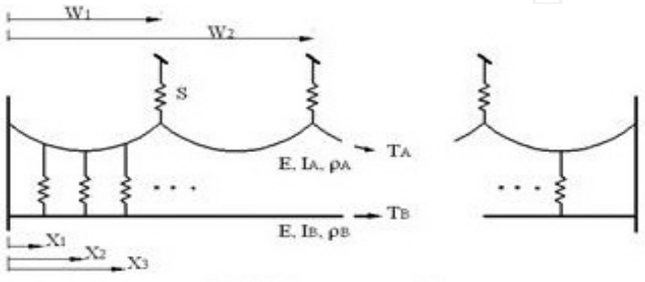

Figure 40. Catenary model

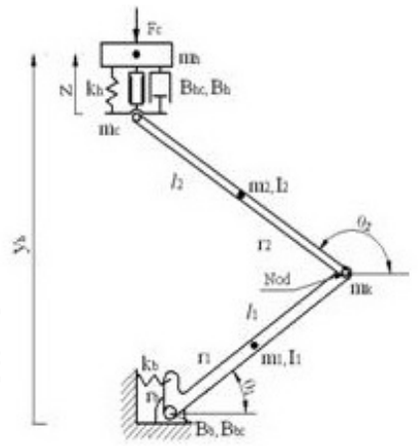

Figure 41. Pantograph model

The equations of motion contain displacement and acceleration terms ($A, \ddot{A}, B, \ddot{B}$). When the system is excited, the catenary's response is harmonic so the acceleration terms are:

$$\ddot{A}_m = -\omega^2 A_m \tag{33}$$

$$\ddot{B}_m = -\omega^2 B_m \tag{34}$$

where: ω - the natural frequency of vibration

The orthogonal modes of the catenary can be considered separately and the result from modal analysis gives the equation for each mode:

$$M_i \ddot{z}_i + 2\xi_i \omega_i M_i \dot{z}_i + \omega_i^2 M_i Z_i = Q_i \tag{35}$$

where: $z_i(t)$ – the i-th model response; m_i – the i-th modal mass; ξ_i - the damping ratio; ω_i – the i-th natural frequency; Q_i – the i-th modal forcing function.

Simulation started at time t=0 seconds with the pantograph at pillar zero, on the contact wire acting the pantograph's lifting force, becoming contact force starting with this moment.

By pantograph's forwarding along the running track, it moves successively the catenary's sections upwards and, thus, induces a vibrating motion of the wire of which oscillations, after pantograph's passing, propagate along the contact wire.

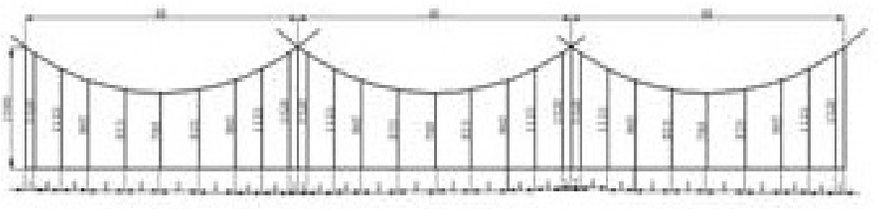

Figure 42. The three spans of the catenary

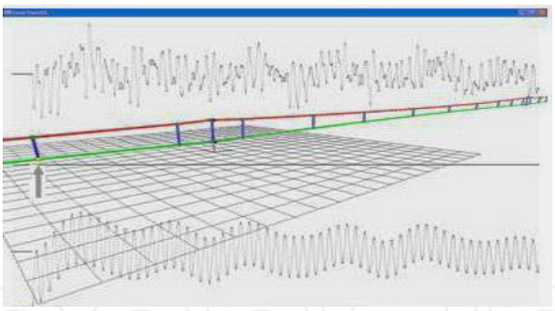

Figure 43. Propagation of the oscillating motion induced by the pantograph's excitation force and catenary's deformation, after t=8,98s

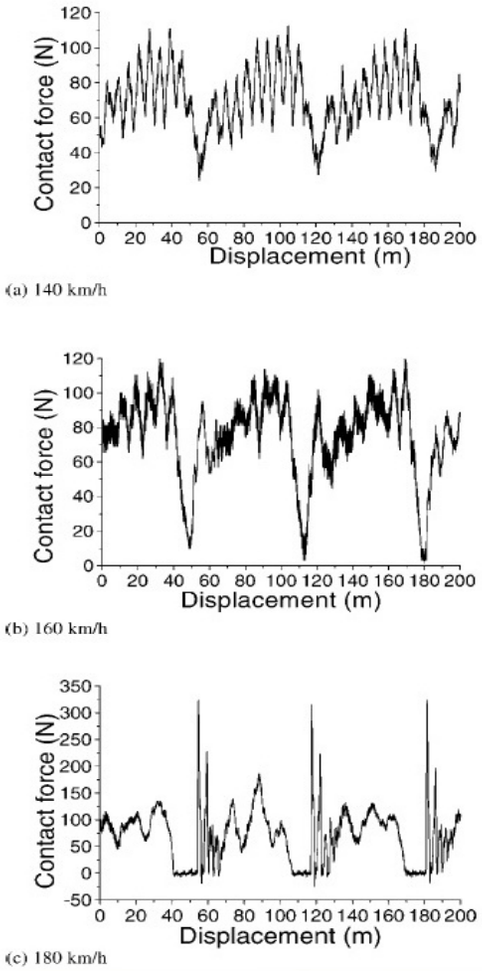

Figure 44. Contact force at different speed

Exemplifying of this phenomenon is shown in fig. 43 that includes also the deformed shape of the catenary suspension, afferent to the pantograph's position right at a node located in the last third of the first span.

The shape shifting of the catenary's distortion right at the pillars (from a steep descent to a slope less pronounced) has the most pronounced effect on the pantograph's performances, the operation data confirming also that in these areas are noticed also the most frequent

contact losses. This conclusion is confirmed also in the specialty literature, the authors finding that at speeds over 150km/h, even the pantograph's crosshead shoe could keep the contact (because the upper suspension, being lighter, could accommodate to a greater movement between the crosshead shoe and the frame), the pantograph's frame responds slower (because, having a greater mass and inertia forces are higher) and, while the pantograph passes the area in the right of a supporting pillar, it sub-vibrates, the result being a smaller contact force.

Table 3 shows the characteristics of contact force at a different speed. It can be seen that with the increasing of speed the characteristics of contact force are getting worse. The speed of 160 km/h is a critical point. At this speed, the contact force approaches to zero. It means that the slipper-shoe of the pantograph lost contact with the overhead line.

Speed (km/h)	100	120	140	160	170	180
Max. contact force (N)	99	103	105	117	119	367
Max. contact force (N)	42	40	24	2	0	0

Table 3. The contact force at different speed

When the running speed is less than this speed, the contact force is larger than zero and the pantograph – catenary system works well. But when the running speed is larger than 160 km/h, loss of contact occurs and becomes more frequent with the increasing of the speed. Considering the minimum contact force should be larger than 20 ~ 30 N in order to keep good contact, we can see from the result that the EP3 pantograph together with the tested catenary, is only suitable for running speed less than 140 km/h. Figure 44 shows the contact force under a speed of 140, 160 and 180 km/h. At a speed of 180 km/h, the contact is lost, and the impact causes large maximum contact force.

3.3. Active control strategies

Studying the previously presented problem, one can observe that the contact force between the pantograph and the catenary is variable, due to a different dynamical behavior of the two parts, with maxima and minima which occur at a frequency of 0.5÷2 [Hz].

For flow speeds over 350km/h, on special lines built and equipped for this purpose, one can find in the literature active control solutions of contact force through "classical" methods [22] [23] [24] [25] [26] or advanced methods [27], [28], [29].

These are quite expensive and not profitable when used at lower speeds (160km/h÷ 220km/h). For this case, we propose a contact force control system of the pantograph-catenary based on the fuzzy logic.

Our aim is to reduce variations in the contact force, by eliminating the pantograph detachment and the appearance of excessive peaks (Table 3), which lead to a premature wear of the contact wire. The structure of the contact force control system is shown in Figure 45.

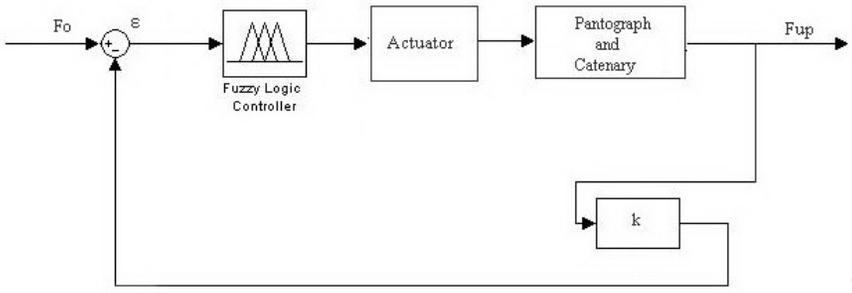

Figure 45. System structure

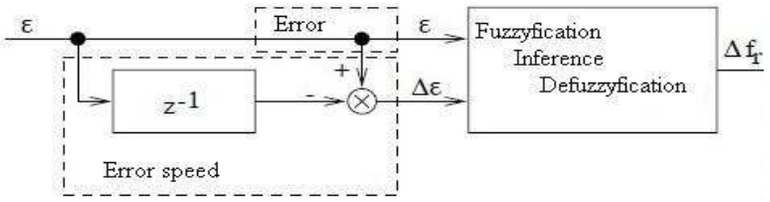

Figure 46. Fuzzy controller

The proposed fuzzy controller presented in Figure 46, will determine the correction through which the contact force will be closer to the desired value, using the information given by the error (ε) and rate of change of the error (Δε).

The variables (ε) and (Δε) are converted into fuzzy variables, using membership functions and the discussion universes in Figures 47, 48 and 49.

The variables (ε) and (Δε) are processed using the inference of the 49 rules (Table 4) through the method of min/max. Output defuzification is made by the centroid method.

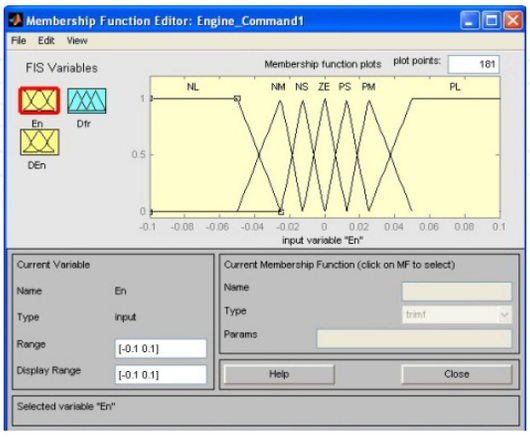

Figure 47. Membership functions for error

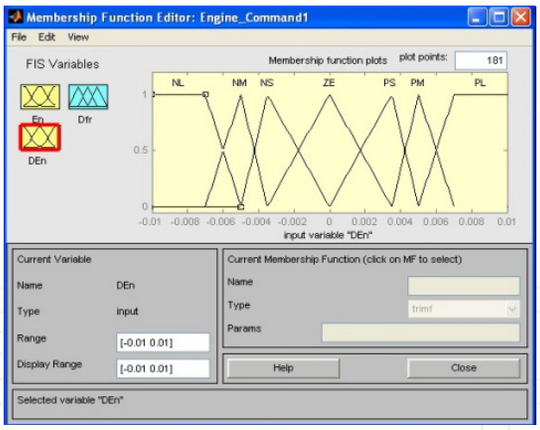

Figure 48. Membership functions for speed error

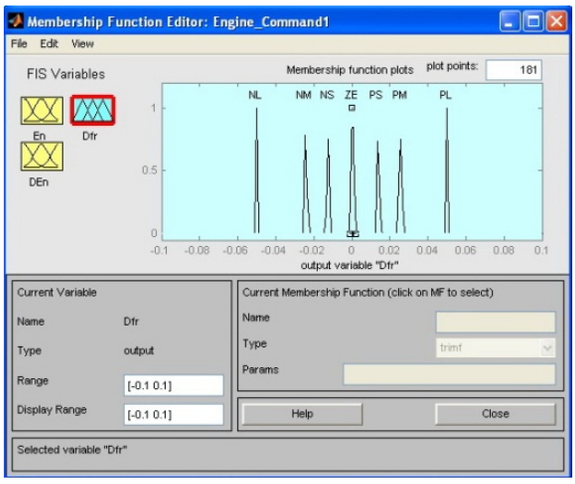

Figure 49. Membership functions for command

Δf_r \ $\Delta \varepsilon_n$	**NL**	**NM**	**NS**	**ZE**	**PS**	**PM**	**PL**
NL	NL	NL	NL	NL	NM	NS	ZE
NM	NL	NL	NL	NM	NS	ZE	PS
NS	NL	NL	NM	NS	ZE	PS	PM
ZE	NL	NM	NS	ZE	PS	PM	PL
PS	NM	NS	ZE	PS	PM	PL	PL
PM	NS	ZE	PS	PM	PL	PL	PL
PL	ZE	PS	PM	PL	PL	PL	PL

Table 4. Rule base

The control area of the proposed fuzzy controller is shown in Figure 50.

Using a Matlab-Simulink simulation, we performed a fuzzy controller functionality simulation. The simulation results are presented in Figures 51, 52 and 53.

For the signal error, a triangular variation was chosen, which went through all of the conversation universe (with a linear increase error from -0.1 to +0.1, followed by a linear decrease to the initial value). The derivative of the error has constant maximum positive values within the first ten seconds and minimum negative values in the next ten seconds.

The command variable follows the base of rules, namely while the error grows, the correction of contact force gets stronger, as there is a non-linear relationship between the two variables, which is in agreement with the experiment.

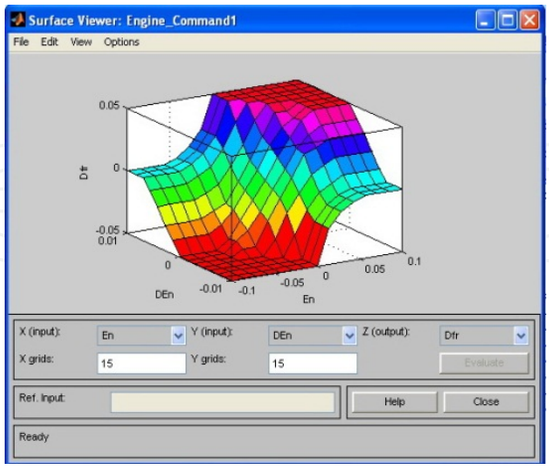

Figure 50. Control surface

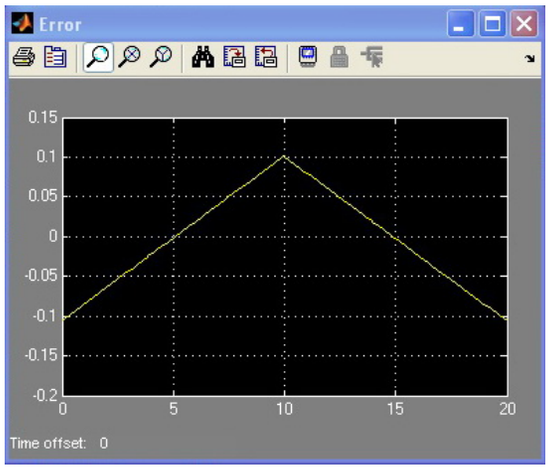

Figure 51. Input signal for error

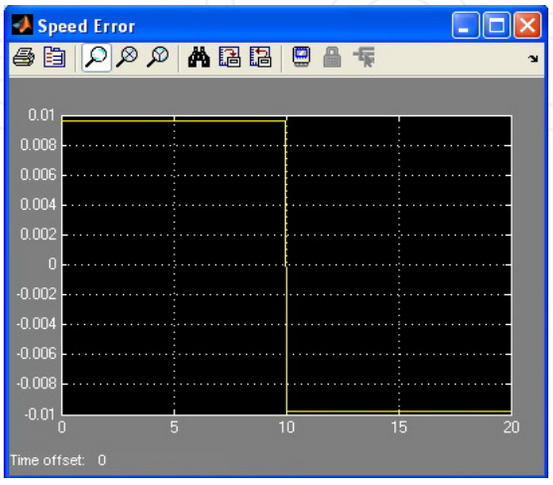

Figure 52. Input signal for speed error

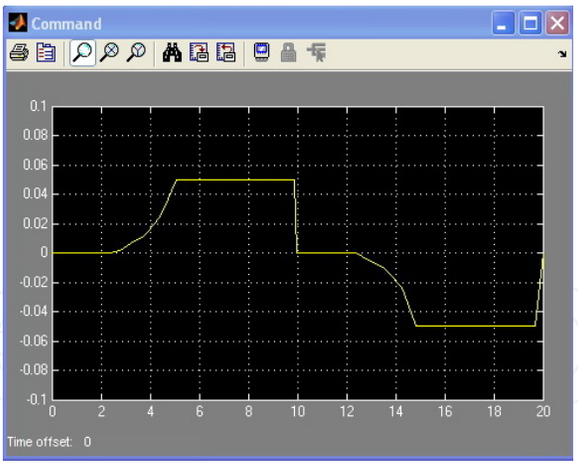

Figure 53. Output signal

When the error changes sign, the strength correction follows the same principle, but in the opposite direction. One concludes that the established rules lead to contact force stabilization. Using the original TENSI-CABLE model and applying the corrections established by the fuzzy system over the dynamic contact force, we were able to estimate the new variation form of the force between the pantograph and the catenary.

Note the small variations ±10N around the value of 75N, which was considered to be the optimal value of the contact force in order to achieve a correct transfer of energy.

The above mentioned variations may be reduced even more in the real implementation phase of the controller, by using a correction of the base of rules.

The speed of response of the control system is very high: only the upper arms have to be moved, reducing the mass to be moved with respect to the case of the force acting of the linkage frame and moving the mass of the whole pantograph. A brushless DC motor with low inertia and small electro-mechanical time constant could be the simplest choice for the electrical actuator.

An important observation must be considered, independently upon the chosen control strategy. In order to overcome the first drawback, the uplift contact force can be subdivised into two terms: a mean term given by a constant force, provided by the traditional passive mechanism (usually a spring or pneumatic cylinder) as in standard pantographs and an additional oscillating term provided by a closed-loop active actuator. In such a way the current collection capability can be maintained even in a case of a failure in the active control apparatus.

A crucial problem to be overcome for a practical implementation of closed-loops active pantograph is the measurement of the contact force. The force sensor must be reliable and lasting in a harsh environment. The traditional solution is to measure the contact force at the support points of the contact strips and to compensate for the inertia of the contact strip by an accelerometer. The required instrumentation is expensive and its life-time is short due to the high temperature and to the vibrational phenomene. Ref [23] presents other methods of simulation for the contact force, which eliminate the previously mentioned disadvantages.

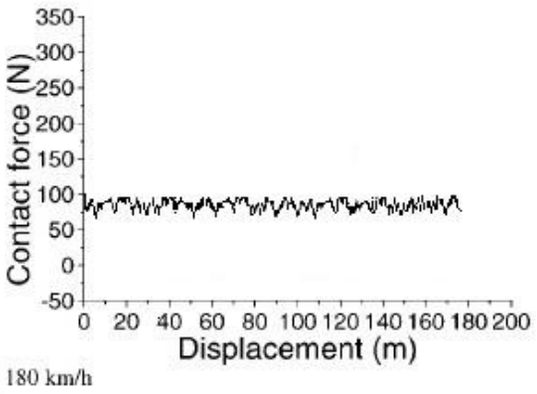

Figure 54. Contact force corrected

4. Conclusion

It can be concluded that usual active harmonic filtering the network side harmonic distortion is reduced very effectively, but the psophometric effect caused by the current along the traction system basically did not change [9]. This situation cannot be tolerated since the effects of induced currents due to the harmonic components and resonance can produce catastrophic effects upon the various equipments placed in the vicinity of the railway power lines.

The proposed Fuzzy DAFS can deploy several small-rated active filter units at various locations within the facility to damp the harmonic resonance. Compared to a centralized, large – rated active filter, the distributed, small-rated active filters with fuzzy logic controlled DAFS can reduce harmonics in the railway power system with improved effectiveness.

The advantage of the presented system based on fuzzy logic is the fact the use of a rather distributed system which is capable to adapt to the railway configuration. Using several filter units, the system has the capability to eliminate harmonic pollution and to avoid harmonic resonance in railway systems. By means using simulation results, we have validating the system considering the coordination of two active filters: one placed in substation area, and the 2nd placed at the end of the line (locomotive level).

Part (B) introduces a complex for the protection of the contact line and of the railway electric transport installations, based on the fuzzy logic. The system we presented has been built in practice and its experimental implementation has shown a series of advantages with respect to the actual systems, such as: low cost; adaptability to any real situation by the appropriate modification of the rules base; very short response time (5μs) of the fuzzy controller; it functionally replaces several protection systems, taking over all their functions. The system has the great advantage over other fuzzy logic relay systems that is designed considering the specific railway power system behavior.

Based on an original numerical model for the dynamical interaction pantograph-catenary, part (C) analyzes the evolution of the contact force between them, concluding that control

could be lost at speeds above 170km/h, with multiple disadvantages. The mathematical model is complex, nonlinear and can not be used directly in managing online the contact force regime. This paper proposes a simple solution based on the fuzzy logic, which eliminates excessive variations, therefore enabling a good electrical contact between the pantograph and the catenary. The system was designed for the traffic of electric locomotives on classical lines, with speeds up to 220 km/h.

Author details

Stela Rusu-Anghel and Lucian Gherman
Politehnica University of Timisoara, Romania

5. References

[1] P. Kiss[1], A. Balogh[2], A. Dan[1], I. Varjasi[2], The Application of Active Filter Supported by Pulse Width Modulated Inverters in the Harmonic Simulation of the High Power Electric Traction , *Proceedings of ICREPQ 2008 – Canary Islands*, pp. 231-236.

[2] Po-Tai Cheng, Zhung-Lin Lee, Distributed Active Filter Systems (DAFS): A new approach to power system harmonics, *The 39th IEEE Conference IAS 2004,* Seattle, USA, pp. 94 – 101.

[3] H. Akagi, Modern active filters and traditional passive filters, *Bulletin of the Polish Academy of Sciences Technical Sciences*, Vol. 54, No. 3, 2006, Warsaw , pp. 255 – 269.

[4] B. Dobrucky, M. Pokorny, V. Racek, R. Havrila, A New Method of the Instantaneous Reactive Power Determination for Single-Phase Power Electronics Systems, *Proceedings EPE 2003 Lausanne* , pp. 1 – 9.

[5] Juraj Altus[1)], Jan Michalik[1)], Branislav Dobrucky[1)], L.H. Viet[2)], Single-Phase Power Active Filter Using Instantaneous Reactive Power Theory – Theoretical and Practical Approach, *Journal of Electrical Power Quality and Utilization,* Vol. 11, No. 1, 2005, pp. 33 – 38.

[6] Ahmed A. Helal, Nahla E. Zakzouk, and Yasser G. Desouky, Fuzzy Logic Controlled Shunt Active Power Filter for Three-phase Four-wire Systems with Balanced and Unbalanced Loads, *Proceedings World Academy of science, Engineering and Technology 58 2009*, ISSN 2070 - 3740, pp. 621 – 627.

[7] Soumia Kerrouche, Fateh Krim, Three-phase Active Filter Based on Fuzzy Logic Controller, *International Journal of Sciences and Techniques of Automatic Control & computer engineering IJ-STA,* Vol. 3, No. 1, 2009, pp. 942 – 955.

[8] Victor M. Moreno[1], Alberto Pigazo[1], Improved Injection Current Controller in Single-Phase Shunt Active Power Filters, *International Conference on Renewable Energy and Power Quality ICREPQ 2005,* Saragossa, Spain

[9] Hideaki Fujita, Takahiro Yamasaki, Hirofumi Akagi, A Hybrid Active Filter for Damping of Harmonic resonance in Industrial Power Systems, *Proceedings IEEE Transactionson Power Electronics*, Vol.15, No.2, March 2000, Japan, pp. 215 – 222.

[10] S. Rusu – Anghel and others, "Advanced System for the Control of Work Regime of Railway Electric Drive Equipment", Contract research no. 53/2009, Politehnica University of Timisoara – SC. SOFTRONIC S.A. Craiova, Romania, 2009.

[11] Popovic, T. Kuhn, M. "Automated fault analysis: From requirements to implementation", Power & energy Society General Meeting, 2009. PES '09. IEEE, pp 1 – 6, 2009, Calgary, AB.

[12] Saleem, A.Z. ; Khan, Z.A. ; Imran, A. "Algorithms and hardware design of modern numeric overcurrent and distance relays", Electrical Engineering, 2008. ICEE 2008. Second International Conference on IEEE, pp 1 – 5, 2008, Lahore.

[13] Soliman, W.M. ; Soudy, B.E.-D.H. ; Wahab, M.A.A. ; Mansour, M.M. "Power generation station faults diagnosis based on fuzzy relations using information of protective relays and circuit breakers", Electric Power and Energy Conversion Systems, 2009. EPECS '09. International Conference on IEEE, pp 1 – 6, 2010, Sharjah.

[14] Farzad Zhalefar, Majid Sanaye-Pasand, "A new Fuzzy-logic-based Extendet Blocking Scheme for Differential Protection of power Transformers", Control and Intelligent Processing Center of Excellence, School of Electrical and Computer Engineering, University of Tehran, Tehran, Iran, Eds. Taylor & Francis, vol 38, pp 675-694, 2010.

[15] Hubertus, J ; Mooney, J ; Alexander, G. "Application Considerations for Distance Relays on Impedance-Grounded Systems", Protective Relay Engineers, 2008 61st Annual Conference for IEEE, pp 196-203, 2008, College Station, TX.

[16] Youssef, O.A.S. "Applications of fuzzy inference mechanisms to power system relaying" Power Systems Conference and Exposition, 2004. IEEE PES, vol 1, pp 560 – 567, 2005.

[17] Spectrum Digital Inc, Application Note The Design and Development of Fuzzy Logic Controllers, 2009.

[18] N. Rusu, J. Averseng, C. Miklos, C. Alic, S. Anghel "Dynamic Modeling of Pantograph – Catenary System for Energy Loss Control" Conference on Automation, Quality and Testing, Proceedings of AQTR-IEEE, vol III pp 11 – 14, Cluj-Napoca, Romania, 2006.

[19] A. Carnicero, J. Simenez, A. Ramos, C. Sanchez "Simulation Models of the Catenary – Pantograph Dynamic Interaction: Validations and Applications " , Proceedings of Power Transmissions in High Speed Railways Systems Seminar, pp 13 – 26, ESIEE – Awiens, France, 2009.

[20] J. Bennet et al, "Advanced Algorithm to Calculate Mechanical Forces on a Catenary", Computers in Railways IX, pp 857 – 868, Germany, 05.2009.

[21] Weihua Zhang et al, "Hybrid Simulation of Dynamics for the Pantograph – Catenary System", Vehicle System Dynamics, Volume 38, Issue 6, Pp 393 – 414, 2002.

[22] M. A. Abdullah, Y. Michitsuji, M. Nagai, N. Miyajima, "Integrated Simulation between Flexible Body of Catenary and Active Control Pantograph for Contact force Variation Control", Journal of Mechanical Systems for Transportation and Logistics, Vol 3, No. 1, 2010 pp 166 – 177 .

[23] G. Diana, F. Fossati, F. Resta, "High Speed Railway: Collecting Pantographs Active control and Overhead Lines Diagnostic Solutions", Vehicle System Dynamics, Volume 30, Issue 1, pp 69 – 84, 1998.

[24] D.N. O'Connor, S.D. Eppinger, W.P. Seering, D.N. Wormley, "Active Control of a High-Speed Pantograph", Journal of Dynamic Systems, Measurement, and Control, Vol 119, pp 1 - 4, March 1997

[25] A. Balestrino, O. Bruno, A. Landi, L. Sani, "Innovative Solutions for Overhead Catenary-Pantograph System : Wire Actuated control and Observed Contact Force", Vehicle System Dynamics, Volume 33, Issue 2, pp 69 – 89, 2000.

[26] A. Levant, A. Pisano, E. Usai, "Output-Feedback Control of the Contact Force in High-Speed-Train Pantographs", Proceedings of the 40th IEEE Conference on Decision and Control, pp 1831 – 1836, Orlando, Florida USA, December 2001.

[27] B. Allotta, A. Pisano, L. Pugi, E. Usai, "VSC of servo-actuated ATR90-type pantograph", Proceedings of the 44th IEEE Conference on Decision and the european Control Conference 2005, pp 590 - 595, Seville, Spain, December 2005.

[28] Y. J. Huang, "Discrete fuzzy variable structure control for pantograph position control", Electrical Engineering 2004, No 86, pp 171 – 177.

[29] Y. J. Huang, T. C. Kuo, "Discrete Pantograph Position Control for the High Speed Transportation Systems", Proceedings of the 2004 IEEE International Conference on Networking, Sensing & Control Taipei, Taiwan, pp 21 – 23, March, 2004.